Available online at www.sciencedirect.com
ScienceDirect
Journal of Sound and Vibration 320 (2009) 254–272
JOURNAL OF SOUND AND VIBRATION
www.elsevier.com/locate/jsvi

Dynamic modeling and stability analysis of an axially oscillating beam undergoing periodic impulsive force

Hong Hee Yoo[a,*], Sung Do Kim[b,1], Jintai Chung[c,2]

[a]School of Mechanical Engineering, Hanyang University, 17 Haengdang-Dong Sungdong-Gu, Seoul 133-791, South Korea
[b]Chassis Engineering Team 1, Hyundai-KIA Motor Company, Jangduk-Dong 772-1, Hwaseong-Si, Gyeonggi-Do 445-706, South Korea
[c]Department of Mechanical Engineering, Hanyang University, 1271 Sa-1-Dong, Ansan, Kyunggi-Do 425-791, South Korea

Received 1 May 2008; received in revised form 22 July 2008; accepted 25 July 2008
Handling Editor: J. Lam
Available online 19 September 2008

Abstract

A dynamic modeling method of an axially oscillating beam undergoing periodic impulsive force is proposed in the present work. An element-specific modeling method using a stretch deformation variable is employed to derive the linear equations of motion. The stiffness variation effect induced by the periodic impulsive force as well as the axially oscillating motion is included in the linear equations of motion. The accuracy of the proposed modeling method is verified by comparing its numerical solutions to those of a nonlinear finite element code. The effects of the impulse magnitude, the oscillating frequency, the oscillating speed amplitude and the modal damping ratio on the dynamic stability of the beam are investigated with the modeling method.

1. Introduction

The axially oscillating motion of a cantilever beam results in bending stiffness variation. If a cantilever beam accelerates toward its free end, the bending stiffness decreases due to compression. However, if the cantilever beam accelerates toward its fixed end, the bending stiffness increases due to stretching. Therefore, the axially oscillating motion of a cantilever beam results in an oscillating time-varying bending stiffness. The oscillating stiffness can cause unstable resonance-like phenomena, which differ from normal resonance, in certain frequency ranges. Such a system with oscillating time-varying stiffness is called a parametrically excited system and the resonance-like phenomena are called parametric resonance.

The needle of a high-speed sewing machine is a typical example of a cantilever beam undergoing axially oscillating motion. The average operating speed of the latest high-speed sewing machine is around 3000–4000 rev/min with the maximum speed often reaching 10,000 rev/min. The needle's bending stiffness of a high-speed sewing machine is designed considerably high. Therefore, unless the needle is improperly designed,

*Corresponding author. Tel.: +82 2 2220 0446; fax: +82 2 2293 5070.
E-mail addresses: hhyoo@hanyang.ac.kr (H.H. Yoo), zzaa@hyundai-motor.com (S.D. Kim), jchung@hanyang.ac.kr (J. Chung).
[1]Tel.: +82 31 368 3370; fax: +82 31 368 3236.
[2]Tel.: +82 31 400 5287; fax: +82 31 406 5550.

0022-460X/$ - see front matter © 2008 Elsevier Ltd. All rights reserved.
doi:10.1016/j.jsv.2008.07.027

an unstable dynamic response of a needle due to normal or parametric resonance rarely occurs. However, if the oscillating frequency needs to be increased for better productivity, the designer of the needle should be careful to avoid parametric resonance phenomena.

When the needle of a high-speed sewing machine penetrates a fabric, it undergoes a periodic impulsive force due to its periodic oscillating motion. Thus, the period of the impulsive force applied to the needle is equal to that of the needle's oscillating motion. For high-speed operation, the impulsive force due to the needle's penetration has a considerable magnitude. The stability characteristics of the needle could be significantly influenced by the periodic impulsive force as well as the axially oscillating motion. Therefore, the impulsive force and the oscillating motion which induce the bending stiffness variation need to be considered simultaneously for the stability analysis of the oscillating needle.

The magnitude of the impulsive force reaches a quite large value within a very short duration, several tens or hundreds of micro-seconds. The abrupt change of the impulsive force often causes serious problems when the equations of motion are solved numerically. Furthermore, the impulsive force usually has a complicated, non-smooth, and even uncertain shape. To obtain the dynamic response effectively during the short duration of the impulsive force, it is desirable to employ an impulse and momentum principle rather than the equations of motion. While the impulsive force is not acting on the system, however, it is desirable to employ the ordinary differential equations of motion.

Study on parametrically excited systems began early in 1831 by Faraday [1], and fundamental mathematical bases to investigate the stability of the parametrically excited system were established in the late 19th century by Mathieu [2] and Hill [3]. More advanced methods such as perturbation methods (for instance, see the work by Nayfeh and Mook [4]) were introduced later to investigate the stability of parametrically excited systems. By employing these methods, principal and combinatory parametric resonance regions could be found effectively. The dynamic stability of a beam undergoing periodic axial force, for instance, was analyzed by Beal [5].

For the modeling of structures undergoing overall motion, a number of structural modeling methods have been proposed. Several nonlinear modeling methods (see, for instance, the works by Christensen and Lee [6] and Simo and Vu-Quoc [7]) were proposed to capture the motion-induced stiffness variation effects. For the parametric excitation problems, nonlinear responses of slender beams carrying a lumped mass were investigated by Zavodney and Nayfeh [8] and Dwivedy and Kar [9,10]. In these works, the translational base motion was prescribed and the governing equations of motion retaining up to cubic nonlinear terms were derived. The method of multiple scales along with the numerical integration technique was employed to analyze the stability of the system. More recently, the combined effect of magnetic field and the periodic axial load was investigated by Pratiher and Dwivedy [11].

Even though many nonlinear models were developed and effectively employed for the stability analysis of a beam undergoing overall base motion, their governing equations were complicated due to the nonlinearity. Moreover, relatively higher computational costs were required for the nonlinear analysis. To overcome the drawbacks of the nonlinear modeling methods, element-specific linear modeling methods were proposed for beams and plates undergoing overall motion by Kane et al. [12], Yoo et al. [13], Seo and Yoo [14], and Yoo and Chung [15]. These modeling methods employ one or two non-Cartesian deformation variables and successfully capture the motion-induced stiffness variation effects. In Refs. [16,17], for instance, the modal characteristics of rotating cantilever beams and rotating cantilever plates were obtained successfully with the linear modeling methods. The modeling method introduced in Ref. [13] was also successfully employed to analyze the stability characteristics of an axially oscillating beam by Hyun and Yoo [18] and a beam with rotary oscillation by Chung et al. [19]. In these works, however, neither the repeated impulsive force effect nor the damping effect on the stability characteristics was investigated.

The purpose of the present study is to propose an accurate and efficient linear modeling method with which the stability of an axially oscillating beam undergoing periodic impulsive force can be effectively analyzed. The stiffness variation effect induced by the periodic impulsive force, which has never been studied by previous researchers so far, is the key ingredient of the proposed modeling method. To obtain more general conclusions, dimensionless equations of motion are derived and four dimensionless parameters are identified. The effects of the four dimensionless parameters related to the impulse magnitude, the oscillating frequency, the oscillating speed amplitude and the modal damping ratio on the dynamic stability of the beam are investigated numerically. The accuracy of the linear modeling method is verified with a comparison study.

2. Derivation of the equations of motion

Fig. 1 shows a cantilever beam attached to a rigid base A^* (the attached point is O) that undergoes an axially oscillating harmonic motion. The beam is characterized by length L, cross sectional area A, area moment of inertia I, Young's modulus E, and mass per unit length ρ. A periodic impulsive force is applied to the free end (point Q) of the beam and the period of the force is same as that of the oscillating motion. If the first impulsive force is applied at $t = 0$, the repeated impulsive force can be expressed as $\sum_{k=0}^{\infty} I_0 \delta(t - kt_I)$ where I_0 and δ respectively denote the impulse generated by the impulsive force and the Dirac delta function. The magnitude of the Dirac delta function remains zero unless t is equal to kt_I where t_I denotes the period of the impulsive force and k denotes an integer number. The elastic displacement of a generic point P of the beam can be expressed by two Cartesian deformation variables u_1 and u_2. In the present work, however, the equations of motion are derived by employing a non-Cartesian deformation variable s representing the stretch along the beam axis. The stretch deformation variable s along with the bending deformation variable u_2 is approximated as follows:

$$s = \sum_{i=1}^{\mu_1} \phi_{1i}(x) q_{1i}(t) \tag{1}$$

$$u_2 = \sum_{i=1}^{\mu_2} \phi_{2i}(x) q_{2i}(t) \tag{2}$$

where $\phi_{1i}(x)$ and $\phi_{2i}(x)$ denote the mode functions for s and u_2; $q_{1i}(t)$ and $q_{2i}(t)$ denote the generalized coordinates; and μ_1 and μ_2 denote the numbers of the generalized coordinates $q_{1i}(t)$ and $q_{2i}(t)$, respectively.

The velocity of the generic point P can be obtained as follows:

$$\vec{v}^P = (v_1 + \dot{u}_1)\hat{a}_1 + \dot{u}_2\hat{a}_2 \tag{3}$$

where v_1 represents the axially oscillating speed of point O, which can be expressed as

$$v_1 = v \sin \omega t \tag{4}$$

where v and ω denote the amplitude and the frequency of the oscillating motion.

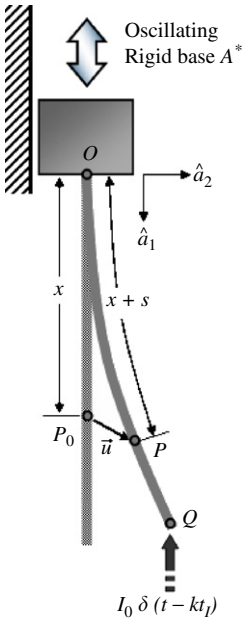

Fig. 1. Configuration of an axially oscillating cantilever beam.

Since u_1 is not employed for the assumed mode approximation, $\dot{u}_1$ in Eq. (3) should be substituted by $\dot{s}$ and $\dot{u}_2$. The following geometric relation can be employed for the purpose:

$$x+s=\int_0^x\left[\left(1+\frac{\partial u_1}{\partial\zeta}\right)^2+\left(\frac{\partial u_2}{\partial\zeta}\right)^2\right]^{1/2}\mathrm{d}\zeta \tag{5}$$

where ζ denotes a dummy variable used for the integral. Using Taylor's series expansion (considering up to the second degree terms), the above equation can be approximated as

$$s\approx u_1+\frac{1}{2}\int_0^x\left(\frac{\partial u_2}{\partial\zeta}\right)^2\mathrm{d}\zeta \tag{6}$$

Therefore the velocity of the generic point P can be expressed as follows:

$$\vec{v}^P=\left[v\sin\omega t+\dot{s}-\int_0^x\left(\frac{\partial u_2}{\partial\zeta}\right)\left(\frac{\partial\dot{u}_2}{\partial\zeta}\right)\mathrm{d}\zeta\right]\hat{a}_1+\dot{u}_2\hat{a}_2 \tag{7}$$

By employing Eq. (7), the partial derivatives of $\vec{v}^P$ with respect to the generalized speeds $\dot{q}_{1i}$ and $\dot{q}_{2i}$ can be obtained as follows:

$$\frac{\partial\vec{v}^P}{\partial\dot{q}_{1i}}=\phi_{1i}\hat{a}_1,\quad \frac{\partial\vec{v}^P}{\partial\dot{q}_{2i}}=-\left[\sum_{j=1}^{\mu_2}\int_0^x(\phi_{2i,\zeta}\phi_{2j,\zeta})\,\mathrm{d}\zeta q_{2j}\right]\hat{a}_1+\phi_{2i}\hat{a}_2 \tag{8}$$

Now linearizing Eq. (7) and differentiating the linearized equation with respect to time, the linearized acceleration of the generic point P can be obtained as follows:

$$\vec{a}^P=(v\omega\cos\omega t+\ddot{s})\hat{a}_1+\ddot{u}_2\hat{a}_2 \tag{9}$$

If Kane's method [20] is employed, the equations of motion can be obtained with the following equation:

$$F_i+F_i^*=0\quad(i=1,2,\ldots,\mu_1+\mu_2) \tag{10}$$

Employing the Euler–Bernoulli beam theory, where the rotary inertia effects are ignored, the generalized inertia forces F_i^* can be obtained with the following equation:

$$F_i^*=-\int_0^L\rho\vec{a}^P\cdot\frac{\partial\vec{v}^P}{\partial\dot{q}_i}\mathrm{d}x \tag{11}$$

where $\dot{q}_i$ consists of $\dot{q}_{1i}$ and $\dot{q}_{2i}$. Considering only stretching and bending effects, the strain energy of a cantilever beam can be expressed as follows:

$$U=\frac{1}{2}\int_0^L EA\left(\frac{\partial s}{\partial x}\right)^2\mathrm{d}x+\frac{1}{2}\int_0^L EI\left(\frac{\partial^2u_2}{\partial x^2}\right)^2\mathrm{d}x \tag{12}$$

The generalized active force F_i consists of F_i^U and F^I which results from the internal strain energy U and the repeated impulsive force, respectively. So,

$$F_i=F_i^U+F_i^I\quad(i=1,2,\ldots,\mu_1+\mu_2) \tag{13}$$

F_i^U and F_i^I can be obtained from the following equations:

$$F_i^U=-\frac{\partial U}{\partial q_i} \tag{14}$$

$$F_i^I=\frac{\partial\vec{v}^Q}{\partial\dot{q}_i}\cdot\left[\sum_{k=0}^{\infty}I_0\delta(t-kt_I)\right]\delta(x-L)\hat{a}_1 \tag{15}$$

Finally, the linearized equations of motion of the axially oscillating beam undergoing periodic impulsive force can be obtained as follows:

$$\sum_{j=1}^{\mu_1}\left[M_{ij}^{11}\ddot{q}_{1j}+K_{ij}^{S}q_{1j}\right]=-v\omega\cos\omega t\,P_i-\sum_{k=0}^{\infty}I_0\delta(t-kt_I)\phi_{1i}(L)\quad(i=1,2,\ldots,\mu_1) \tag{16}$$

$$\sum_{j=1}^{\mu_2}\left[M_{ij}^{22}\ddot{q}_{2j}+\left(K_{ij}^{B}-v\omega\cos\omega\, tK_{ij}^{G}-\sum_{k=0}^{\infty}I_0\delta(t-kt_I)K_{ij}^{I}\right)q_{2j}\right]=0\quad(i=1,2,\ldots,\mu_2) \tag{17}$$

where

$$M_{ij}^{ab}\equiv\int_0^L\rho\phi_{ai}\phi_{bj}\,\mathrm{d}x \tag{18}$$

$$K_{ij}^{S}\equiv\int_0^L EA\phi_{1i,x}\phi_{1j,x}\,\mathrm{d}x \tag{19}$$

$$K_{ij}^{B}\equiv\int_0^L EI\phi_{2i,xx}\phi_{2j,xx}\,\mathrm{d}x \tag{20}$$

$$K_{ij}^{G}\equiv\int_0^L\rho(L-x)\phi_{2i,x}\phi_{2j,x}\,\mathrm{d}x \tag{21}$$

$$K_{ij}^{I}\equiv\int_0^L\phi_{2i,x}\phi_{2j,x}\,\mathrm{d}x \tag{22}$$

$$P_i\equiv\int_0^L\rho\phi_{1i}\,\mathrm{d}x \tag{23}$$

Eqs. (16) and (17) represent the governing equations for stretching motion and bending motion, respectively. Eqs. (16) and (17) are not coupled and the lowest stretching natural frequency is usually far separated from a few lowest bending natural frequencies. So, the stability characteristics of the axially oscillating beam will be investigated by using only Eq. (17). As shown in Eq. (17), there are three stiffness terms: structural stiffness, motion-induced stiffness, and impulse-induced stiffness. This indicates that not only the oscillating motion but also the repeated impulsive force can influence the stability characteristics of the system.

Numerical integration will be employed to obtain the transient response while the impulsive force is not acting. During the short duration of the impulsive force, however, the integration procedure will not be employed. Instead, an impulse and momentum principle will be derived and employed to obtain the numerical solution.

If the eigenfunctions of the beam (with no oscillating motion) are employed as mode functions for Eq. (17), the following equation can be obtained:

$$\ddot{q}_{2i}+\Lambda_i^2q_{2i}-v\omega\cos\omega t\sum_{j=1}^{\mu_2}K_{ij}^{G}q_{2j}-\sum_{k=0}^{\infty}I_0\delta(t-kt_I)\sum_{j=1}^{\mu_2}K_{ij}^{I}q_{2j}=0\quad(i=1,2,\ldots,\mu_2) \tag{24}$$

where Λ_i indicates the ith natural frequency of the stationary beam. Now suppose the first impulse occurs at $t=0$. Since the period of the oscillating motion is equal to that of the impulsive force, Eq. (24) can be rewritten as follows:

$$\ddot{q}_{2i}+\Lambda_i^2q_{2i}-v\omega\cos\omega t\sum_{j=1}^{\mu_2}K_{ij}^{G}q_{2j}-\sum_{k=0}^{\infty}I_0\delta\left(t-\frac{2k\pi}{\omega}\right)\sum_{j=1}^{\mu_2}K_{ij}^{I}q_{2j}=0\quad(i=1,2,\ldots,\mu_2) \tag{25}$$

To obtain more general results and conclusions, Eq. (25) needs to be transformed into a dimensionless form. For the purpose of the transformation, the following dimensionless variables need to be introduced:

$$\xi = \frac{x}{L}, \quad \tau = \frac{t}{T}, \quad \eta_i = \frac{q_{2i}}{L} \tag{26}$$

where

$$T = (\rho L^4/EI)^{1/2}$$

Using the dimensionless variables introduced in Eq. (26), Eq. (25) can be transformed as

$$\ddot{\eta}_i + \omega_i^2 \eta_i - \lambda\gamma \cos \gamma\tau \sum_{j=1}^{\mu_2} \bar{K}_{ij}^G \eta_j - \sum_{k=0}^{\infty} i_0 \delta\left(\tau - \frac{2k\pi}{\gamma}\right) \sum_{j=1}^{\mu_2} \bar{K}_{ij}^I \eta_j = 0 \quad (i = 1, 2, \ldots, \mu_2) \tag{27}$$

where ω_i's denote the dimensionless natural frequencies which can be obtained by multiplying the natural frequencies of the stationary cantilever beam by T and

$$\bar{K}_{ij}^G = \int_0^1 (1-\xi)\psi_{i,\xi}\psi_{j,\xi}\,\mathrm{d}\xi \quad \bar{K}_{ij}^I = \int_0^1 \psi_{i,\xi}\psi_{j,\xi}\,\mathrm{d}\xi \tag{28}$$

$$\lambda = \frac{vT}{L}, \quad \gamma = \omega T, \quad i_0 = \frac{L^2 I_0}{EI} \tag{29}$$

In Eq. (29), λ denotes the dimensionless oscillating speed amplitude, γ denotes the dimensionless oscillating frequency (or the dimensionless impulsive force frequency), and i_0 denotes the dimensionless impulse magnitude.

Now if the damping effect is considered with modal damping model, Eq. (27) can be rewritten as follows:

$$\ddot{\eta}_i + 2\zeta_i\omega_i\eta_i + \omega_i^2 \eta_i - \lambda\gamma \cos \gamma\tau \sum_{j=1}^{\mu_2} \bar{K}_{ij}^G \eta_j - \sum_{k=0}^{\infty} i_0 \delta\left(\tau - \frac{2k\pi}{\gamma}\right) \sum_{j=1}^{\mu_2} \bar{K}_{ij}^I \eta_j = 0 \quad (i = 1, 2, \ldots, \mu_2) \tag{30}$$

where ζ_i denotes the modal damping ratio for the ith natural frequency. The effects of the modal damping ratio and the three dimensionless parameters λ, γ, and i_0 defined in Eq. (29) on the stability characteristics of the axially oscillating cantilever beam will be investigated in the next section.

3. Numerical results

The dynamic stability diagram of an axially oscillating cantilever beam (undergoing no impulsive force) is shown in Fig. 2. The multiple scale perturbation method (see Ref. [4]) considering up to the second-order expansions was employed to obtain the transition curves shown in the figure. The horizontal and the vertical lines of the figure are mainly related to the dimensionless oscillating frequency γ and the dimensionless oscillating speed amplitude λ which were defined in the previous section. As shown in the diagram, many curves originate from several frequencies. The curves originating from $\omega_p + \omega_q$ are called the first-order transition curves and those originating from $(\omega_m + \omega_n)/2$ are called the second-order transition curves. Selection of a point in the diagram determines the stability characteristics of the oscillating beam. If the selected point is located above the transition curves, the response of the oscillating beam will be diverged. For instance, points A and B are located in the stable region and points C, D, E, and F are located in the unstable region.

However, if the oscillating beam undergoes a periodic impulsive force, its stability characteristics can change. Since the stability diagram of the system governed by Eq. (30) cannot be obtained with the multiple scale perturbation method, a direct numerical integration technique along with the impulse and momentum principle is employed to determine the stability.

To verify the accuracy of the present modeling method, the dynamic response results obtained with the present modeling method are compared to those obtained with a nonlinear finite element code (see, Refs. [21,22]). For the finite element code, an impulse is idealized as a half sine function (as shown in Fig. 3), where Δt denotes the duration of the impulsive force and t_I denotes the time to apply the impulsive force. Thus, the

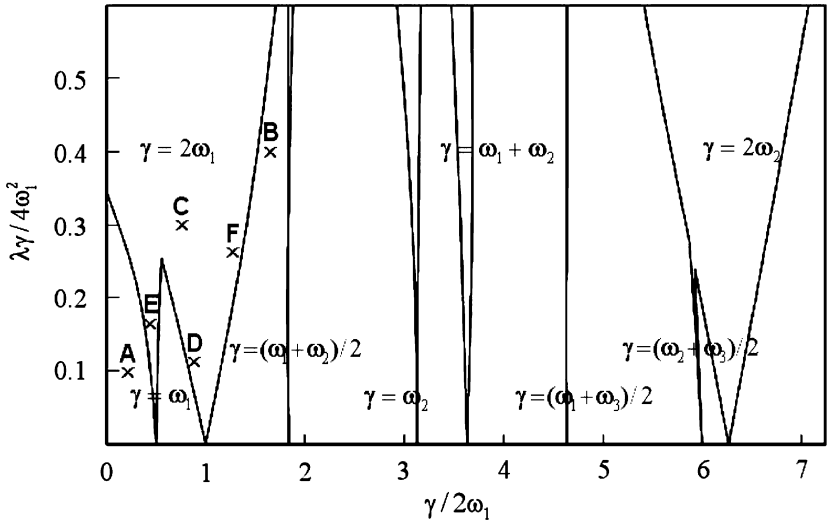

Fig. 2. Stability diagram of the axially oscillating cantilever beam.

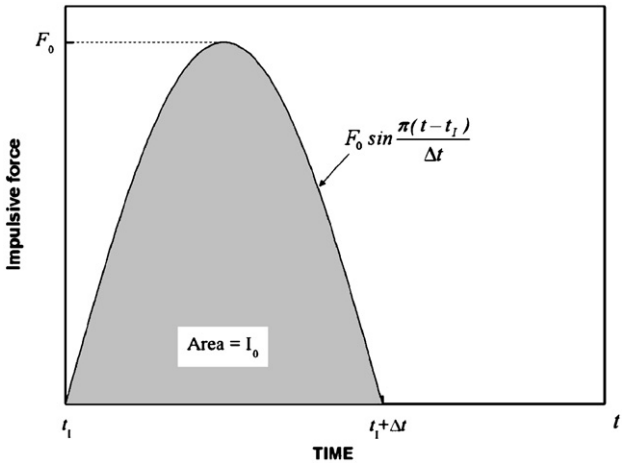

Fig. 3. Function profile of the impulsive force employed for the commercial finite element code.

area of an impulsive force is the amount of impulse I_0 that can be obtained as follows:

$$I_0 = \int_{t_I}^{t_I+\Delta t} F_0 \sin\frac{\pi(t-t_I)}{\Delta t}\,\mathrm{d}t \tag{31}$$

To obtain the dynamic responses, seven bending modes are employed for the present modeling method and ten beam elements are employed for the finite element code. The long term response will be affected by the high-frequency modes as well as the low frequency modes if the damping is not present. However, the high-frequency component will be damped out since the damping always exists in the real physical world. The convergence of the solution was checked out as the number of modes is increased. Since seven bending modes were found to be enough to obtain converged solutions, seven modes were employed in the following numerical results.

The initial values of the displacement (which is assumed to be caused by the first bending mode) and the velocity of the free end of the cantilever beam are given as 1% of the beam length and null, respectively. If a

periodic impulse (which is caused by the repeated impact between the beam tip and an object like a fabric) is applied to the free end point of the oscillating beam, the period of the impulse is equal to that of the oscillating motion. In the following figures, the vertical dotted lines represent the moments at which the repeated impulses are applied to the beam.

The values of λ and γ (corresponding to point A located in the stable region) along with the dimensionless impulse magnitude employed to obtain the results are shown in Fig. 4. The results show that the stability is not much affected by the repeated impulse. Point B is also located in the stable region. As shown in Fig. 5, however, the stability is significantly affected by the repeated impulse. The repeated impulse causes the

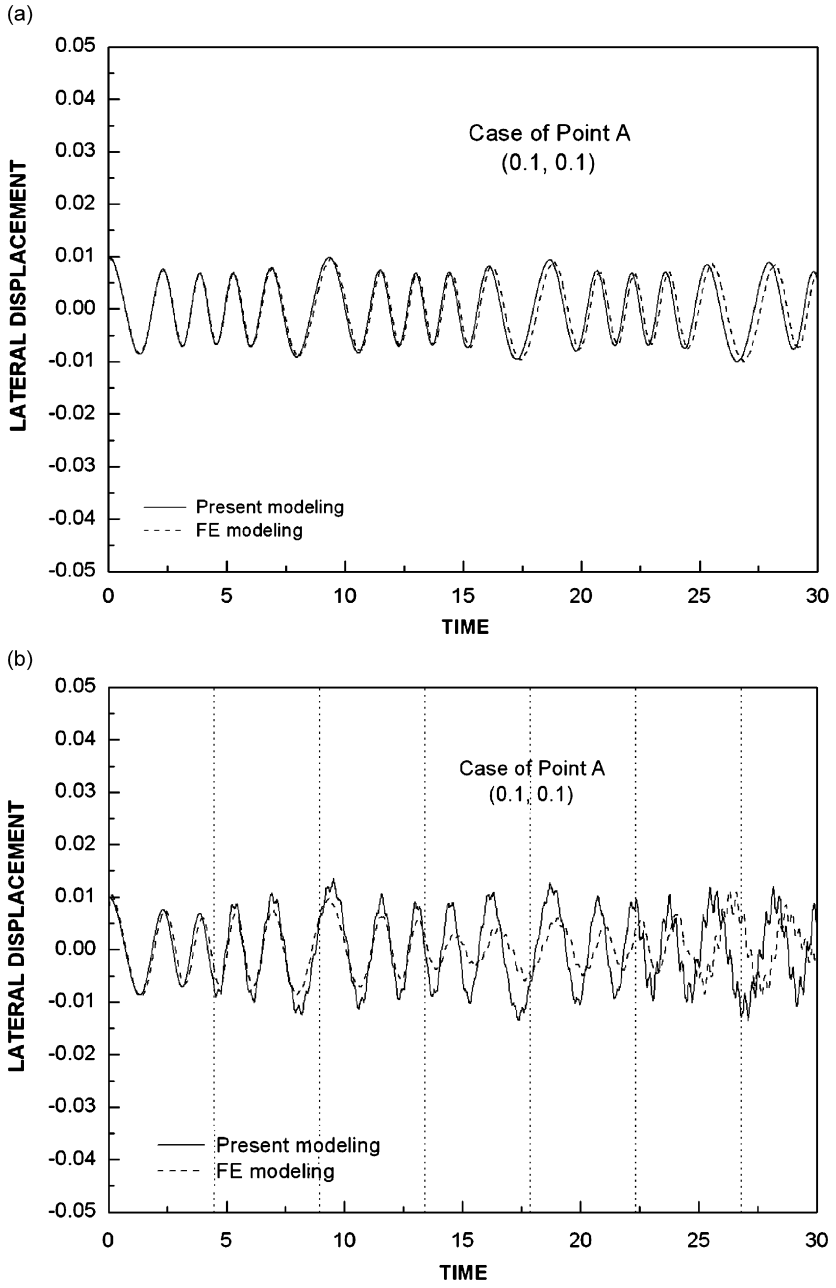

Fig. 4. Comparison of the dynamic response results at point A obtained by the present modeling and the commercial finite element code: (a) $i_0 = 0$ and (b) $i_0 = 1.0$.

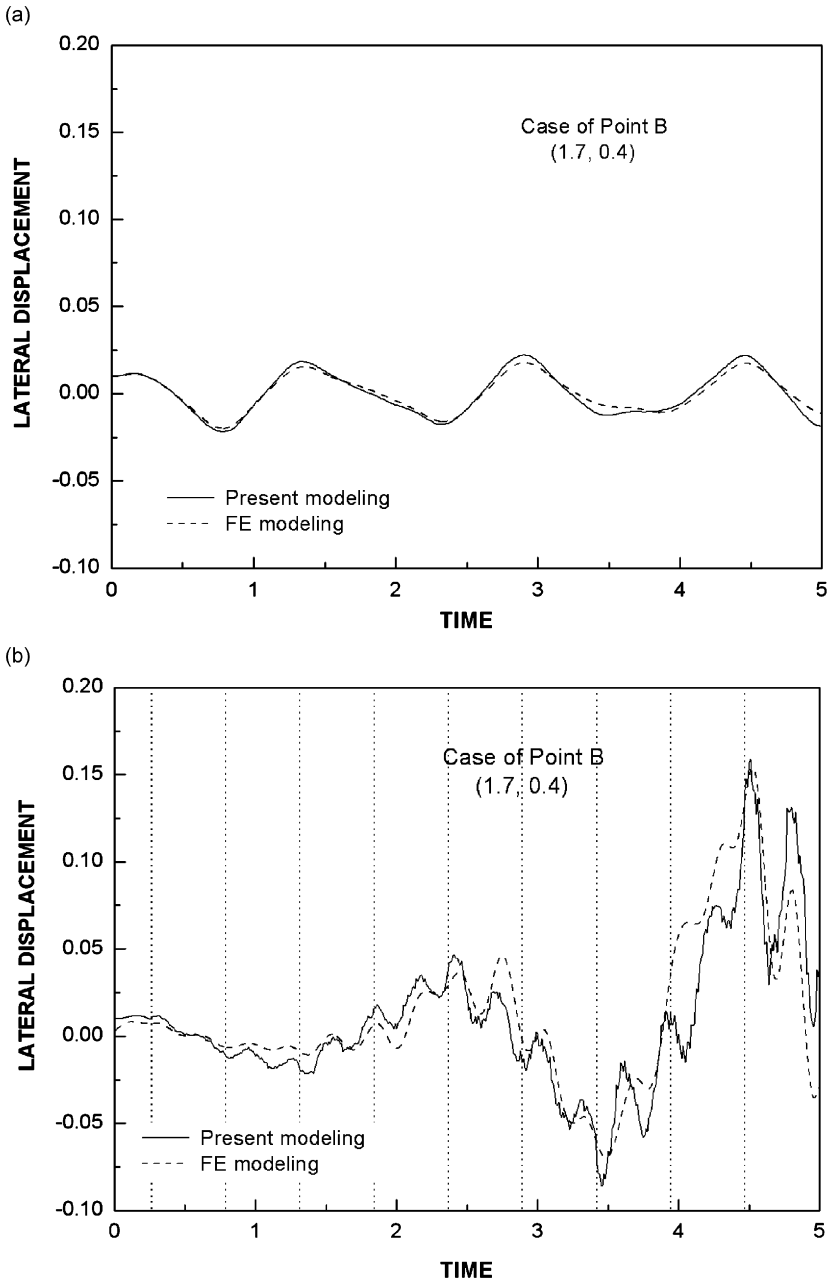

Fig. 5. Comparison of the dynamic response results at point B obtained by the present modeling and the commercial finite element code: (a) $i_0 = 0$ and (b) $i_0 = 1.0$.

unstable response shown in Fig. 5(b). Point C is located in the unstable region. Regardless of the repeated impulse existence, both methods predict diverged responses. Point D is located in the unstable region, too. As shown in Fig. 7(b), however, the repeated impulse results in the stable response. Figs. 4–7 show that the results obtained with the present modeling method are in good agreement with those obtained with the nonlinear finite element code. While the stability diagram (shown in Fig. 2) is plotted basing on the steady-state response of the axially oscillating beam undergoing no repeated impulsive force, Figs. 4–7 show time responses (up to a few periods) which are enough to exhibit the stability of the axially oscillating beam undergoing repeated impulsive force.

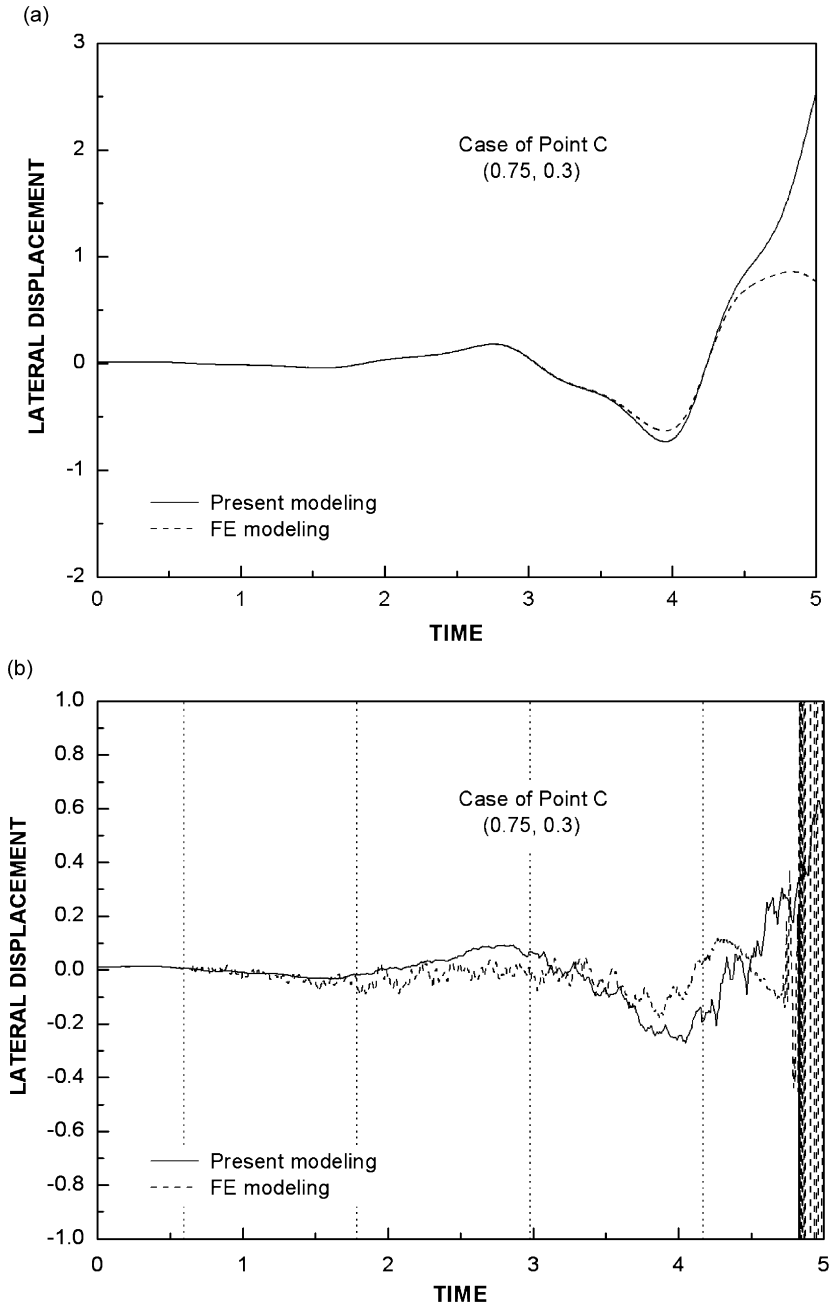

Fig. 6. Comparison of the dynamic response results at point C obtained by the present modeling and the commercial finite element code: (a) $i_0 = 0$ and (b) $i_0 = 1.0$.

Fig. 8 shows the dynamic responses obtained at two points E and F (shown in Fig. 2) by the present modeling method. As shown in Fig. 8(a), the small amount of repeated impulsive force accelerates the diverging trend at point E. On the contrary, at point F, relatively large amount of repeated impulsive force could attenuate the diverging trend to stabilize the system as shown in Fig. 8(b).

The effects of the impulse magnitude, the oscillating speed amplitude and the oscillating frequency on the dynamic stability of the axially oscillating cantilever beam are exhibited in Figs. 9 and 10. Fig. 9 shows the maximum displacement contour map in the plane of the oscillating frequency and the impulse magnitude

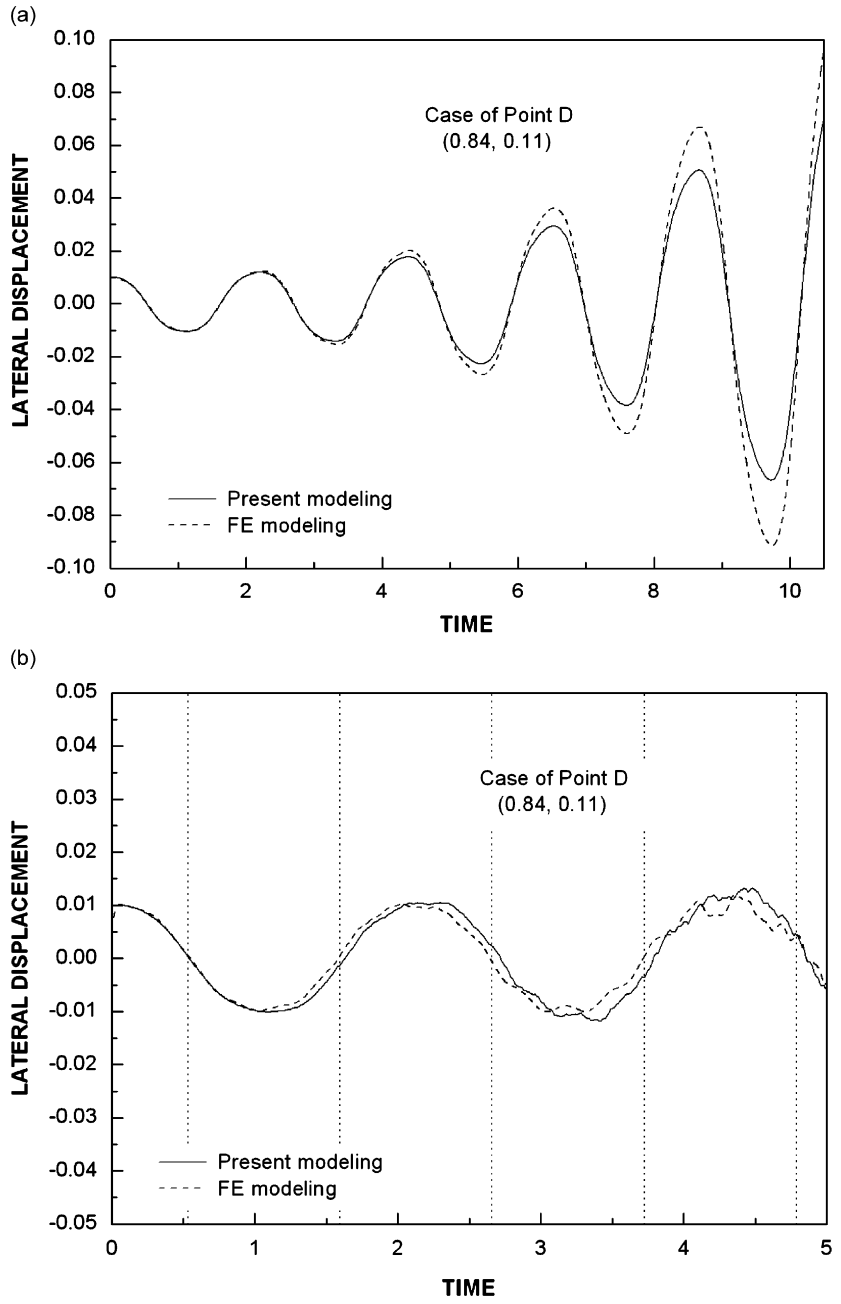

Fig. 7. Comparison of the dynamic response results at point D obtained by the present modeling and the commercial finite element code: (a) $i_0 = 0$ and (b) $i_0 = 0.5$.

obtained by the numerical integration (along with the impulse and momentum principle). The dimensionless oscillating speed amplitude λ and the damping ratio ζ employed to obtain the map are 1 and 0, respectively. Using an ordinary personal computer, numerical integration is performed repeatedly by changing the dimensionless impulse magnitude i_0 and the dimensionless oscillating motion frequency γ to obtain the dimensionless maximum lateral displacement at the free end of the cantilever beam after 10 oscillating motions. It can be shown from the figure that there exists a strong unstable region near $2\omega_1$. In general, if the impulse magnitude is sufficiently large, it will destabilize the system. However, if the impulse magnitude

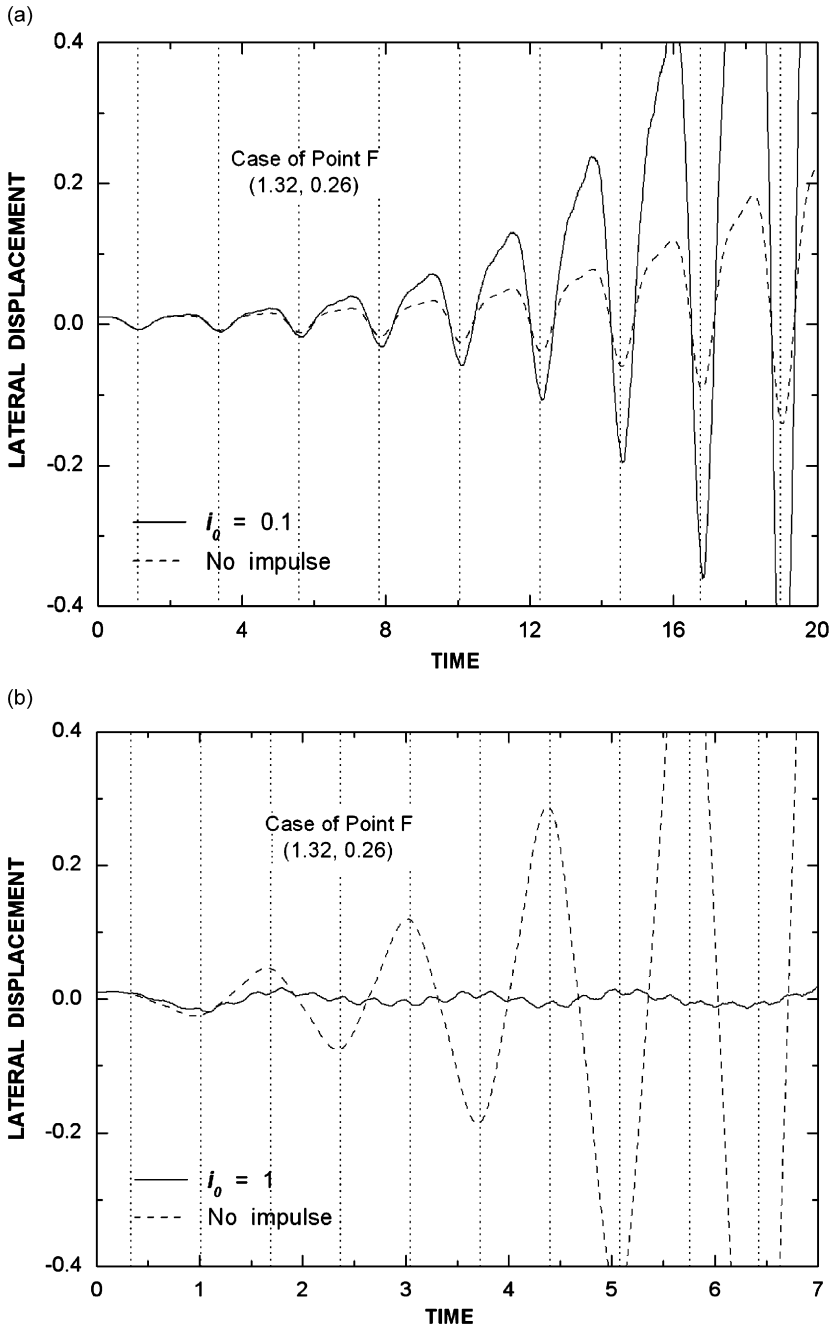

Fig. 8. The repeated impulsive force effect on the dynamic responses at points D and E.

remains proper, the stability can be maintained. For instance, if an impulse magnitude i_0, which is less than 0.4, is imparted, the system remains stable except for the region around $2\omega_1$.

Fig. 10 shows the maximum displacement contour map in the plane of the oscillating speed amplitude and the impulse magnitude. The dimensionless oscillating frequency γ and the damping ratio ζ employed to obtain the map are 10 and 0, respectively. The figure shows that if the oscillation speed amplitude exceeds a certain limit, the system becomes always unstable. However, as mentioned previously, a proper amount of impulse

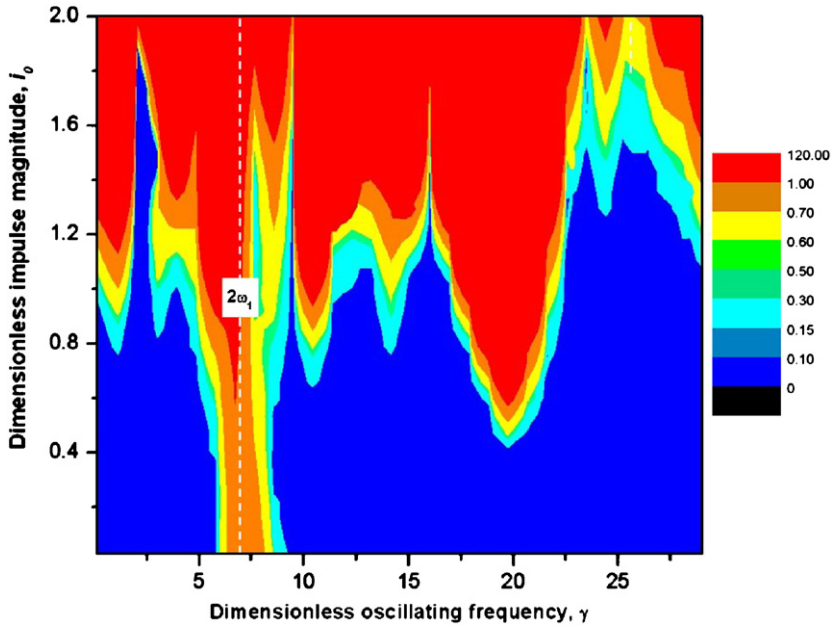

Fig. 9. Maximum displacement contour map in the plane of the oscillating frequency and the impulse magnitude with no damping and $\lambda = 1$.

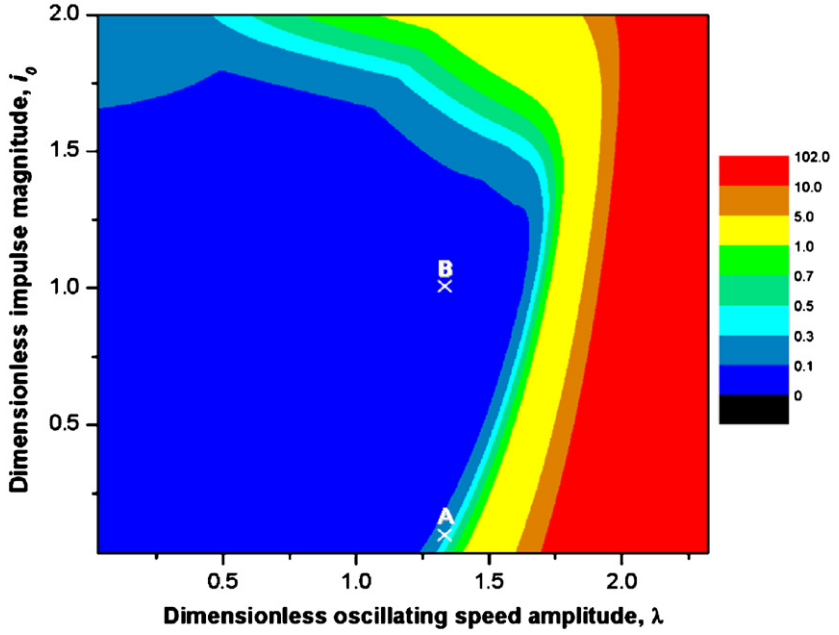

Fig. 10. Maximum displacement contour map in the plane of the oscillating speed amplitude and the impulse magnitude with no damping and $\gamma = 10$.

magnitude can stabilize the system. For instance, Fig. 11 shows the variation of the system response at two points A and B shown in Fig. 10. As shown in Fig. 11, a proper amount of impulse magnitude $i_0 = 1$ (at point B) stabilizes the system response while the less amount of impulse magnitude $i_0 = 0.1$ (at point A) destabilizes the system.

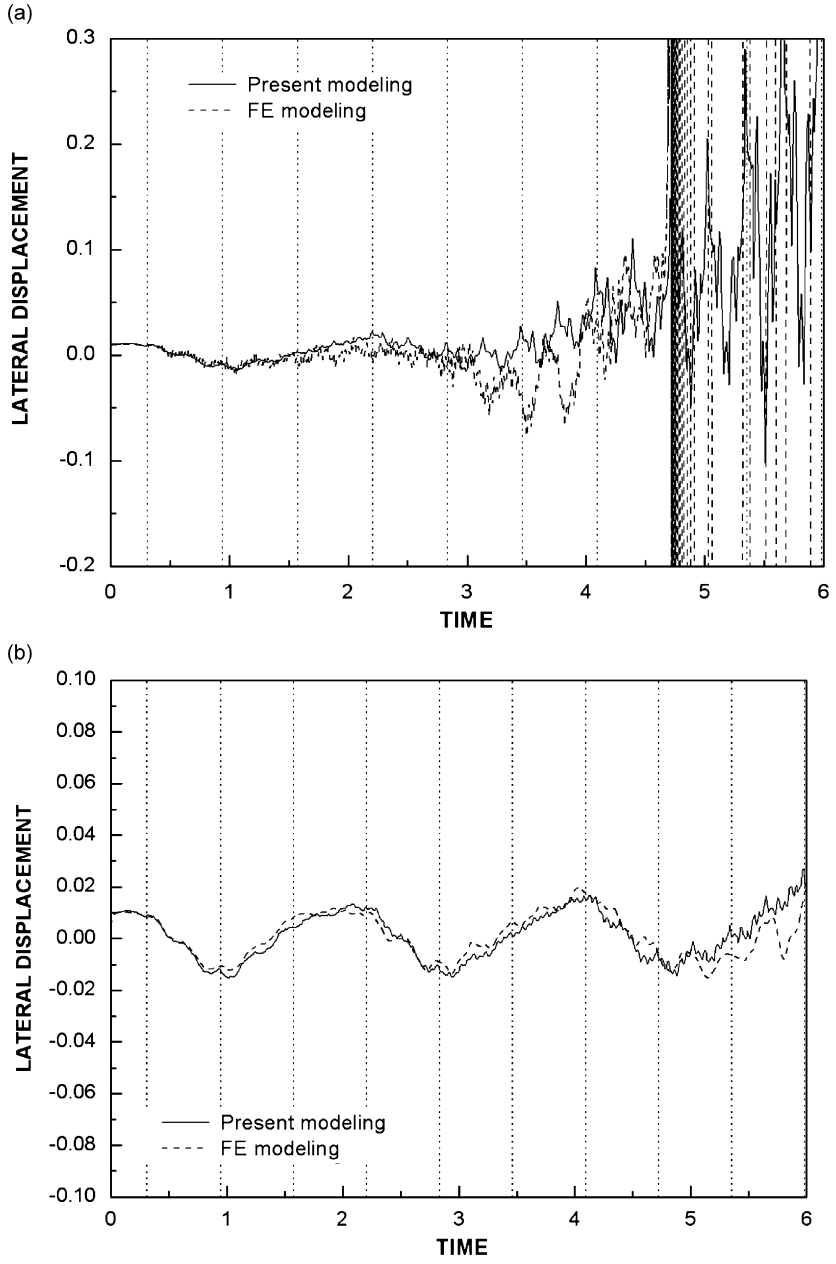

Fig. 11. Impulse magnitude effect on the system response with no damping and $\gamma = 10$: (a) point A (1.3, 0.1) and (b) point B (1.3, 1.0).

To obtain the results shown in the previous figures, no damping effect was considered. To investigate the effect of damping on the stability characteristics of the axially oscillating beam, some modal damping ratios are employed to obtain the results shown in Fig. 12. In the present study, the first two modal damping ratios are set to be same (i.e. $\zeta_1 = \zeta_2 = \zeta$) and determined by the two Rayleigh damping constants α and β. The two Rayleigh damping constants can be used to define a damping matrix as follows: $[C] = \alpha[M] + \beta[K]$. Therefore, the Rayleigh damping constants α and β can be determined by the following equations: $\alpha + \beta\omega_1^2 = 2\zeta\omega_1$ and $\alpha + \beta\omega_2^2 = 2\zeta\omega_2$. Once α and β are determined, other five modal damping ratios are determined by $\alpha + \beta\omega_i^2 = 2\zeta_i\omega_i (i = 3, 4, \ldots, 7)$. The commands of DAMPING_GLOBAL and DAMPING_PART_STIFFNESS are employed in LS-DYNA to define α and β. Comparing to the result shown in Fig. 9, it can be easily

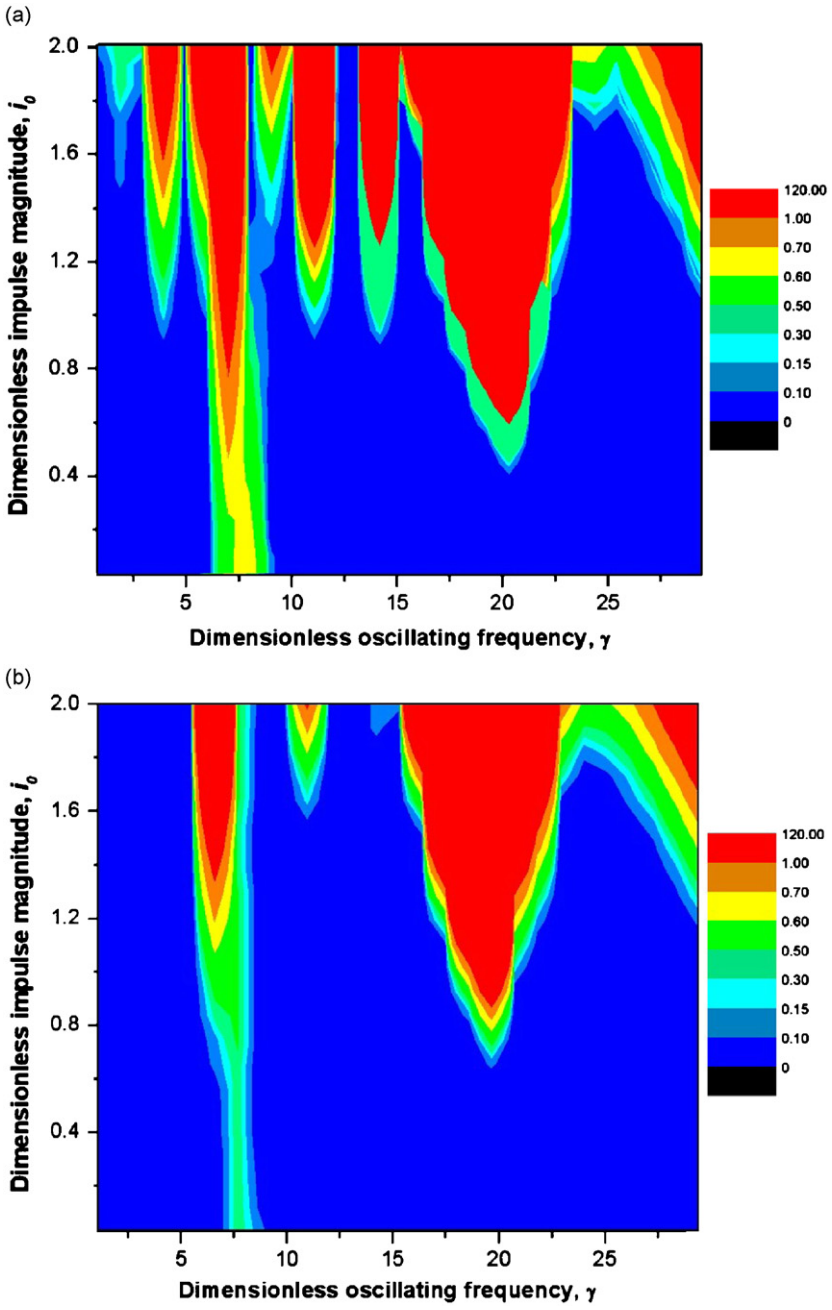

Fig. 12. Maximum displacement contour map in the plane of the oscillating frequency and the impulse magnitude with two damping effects and $\lambda = 1$: (a) $\zeta = 0.1$ and (b) $\zeta = 0.5$.

found that the unstable region decreases as the modal damping ratio increases. Fig. 13 also shows that the unstable region generally decreases as the damping ratio increases. However, even with a large damping ratio ($\zeta = 0.5$ is practically large), the system becomes unstable as the oscillating speed amplitude exceeds a certain limit. Again, the benefit of imparting a repeated impulse can be observed in Fig. 13. As the oscillating speed amplitude λ exceeds a certain value (for instance, approximately 1.3 when $\zeta = 0.1$) and increases, the impulse magnitude i_0 should be also increased to stabilize the system. In Fig. 13(a), points B and D are stable while

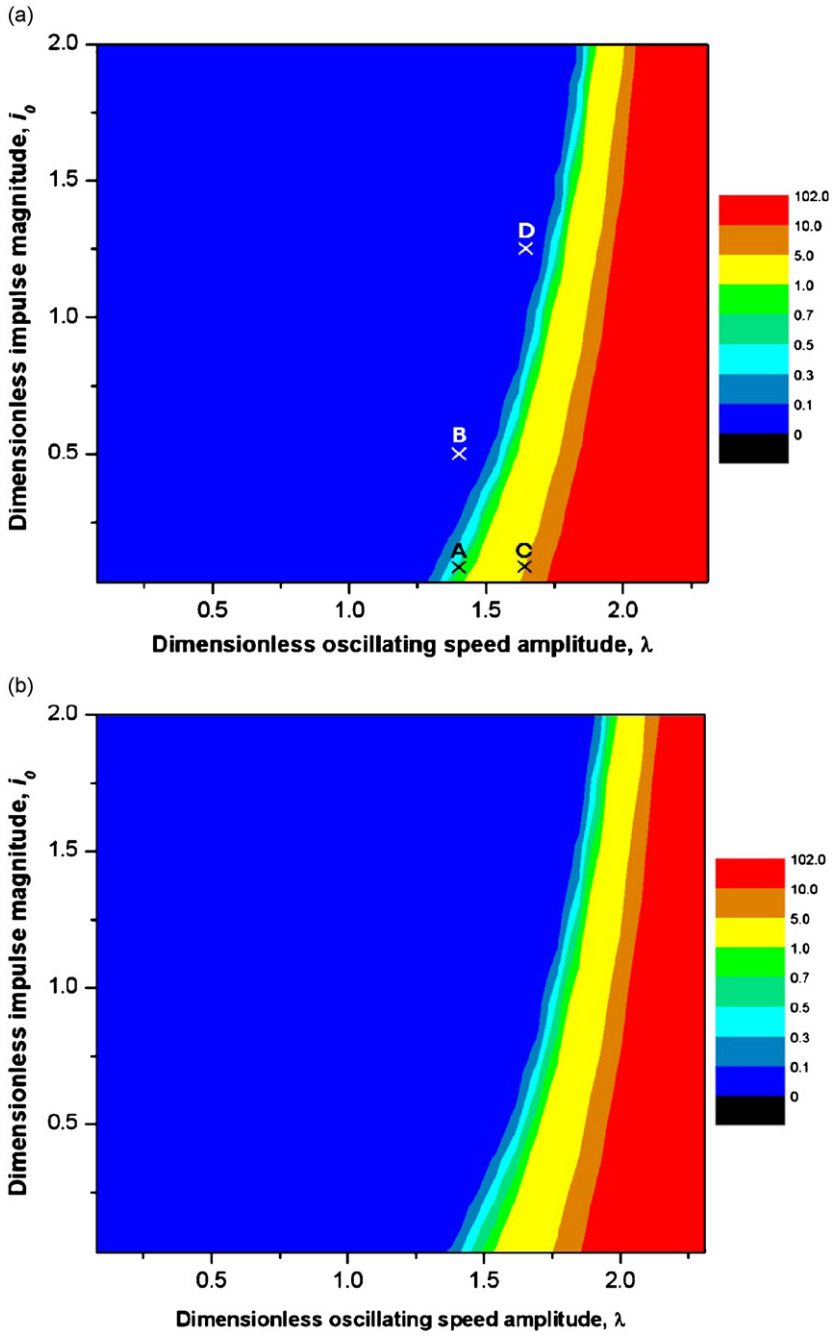

Fig. 13. Maximum displacement contour map in the plane of the oscillating speed amplitude and the impulse magnitude with two damping effects and $\gamma = 10$: (a) $\zeta = 0.1$ and (b) $\zeta = 0.5$.

points A and C are unstable. Figs. 14 and 15 show the system responses at points A, B, C and D shown in Fig. 13(a). As clearly shown in the results, the impulse magnitude i_0 should be increased to stabilize the system as the oscillating speed amplitude λ increases. Comparing to Fig. 10, one can also see that the upper limit of the impulse magnitude to maintain the stability can be extended with the increased modal damping ratio.

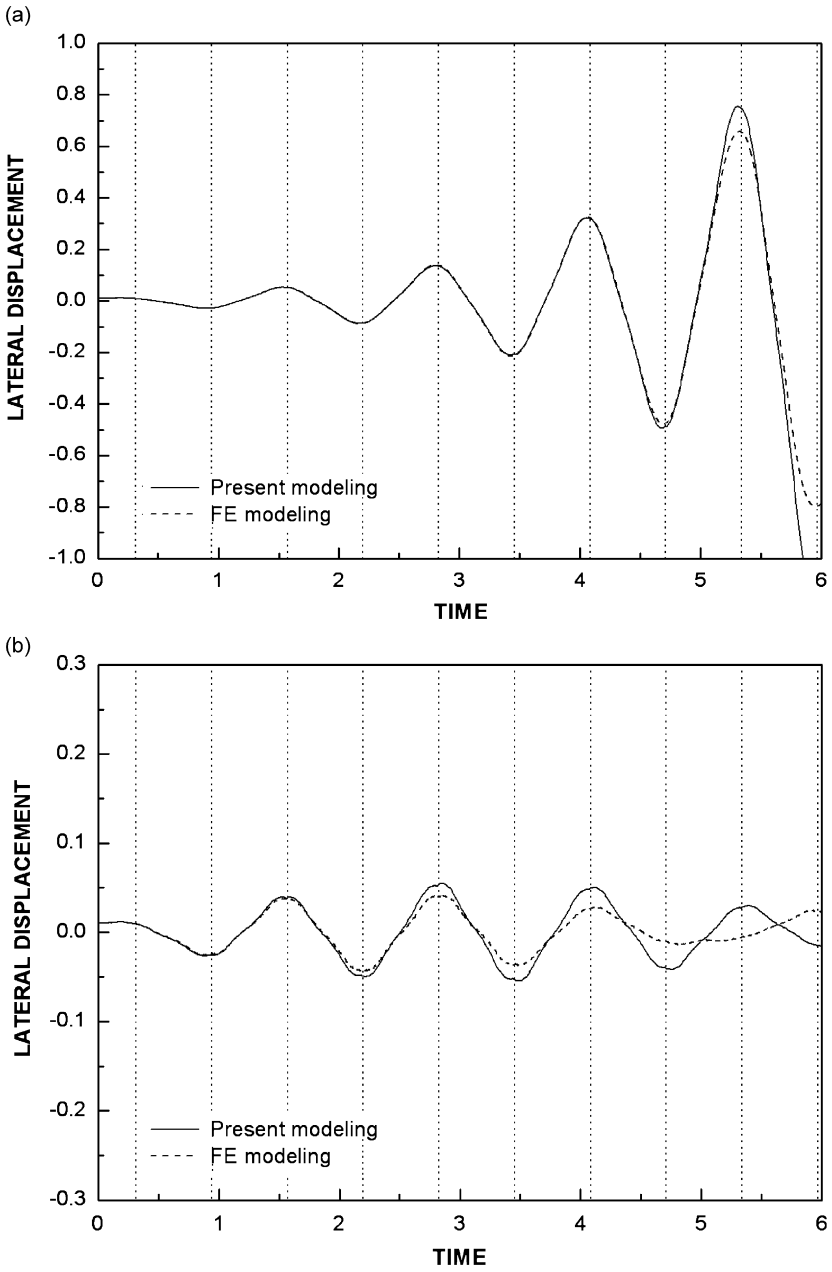

Fig. 14. Impulse magnitude effect on the system response at points A and B (shown in Fig. 13) with $\zeta = 0.1$ and $\gamma = 10$: (a) point A (1.40, 0.10) and (b) point B (1.40, 0.50).

4. Conclusion

A linear computational model to analyze the stability characteristics of an axially oscillating beam undergoing repeated impulsive force is proposed in this study. The proposed model shows that not only the oscillating motion but also the repeated impulsive force can significantly influence the stability of the axially oscillating beam. By employing a nonlinear finite element code, the accuracy of the proposed model is verified. The effects of the repeated impulse magnitude, the oscillating speed amplitude, the oscillating frequency, and

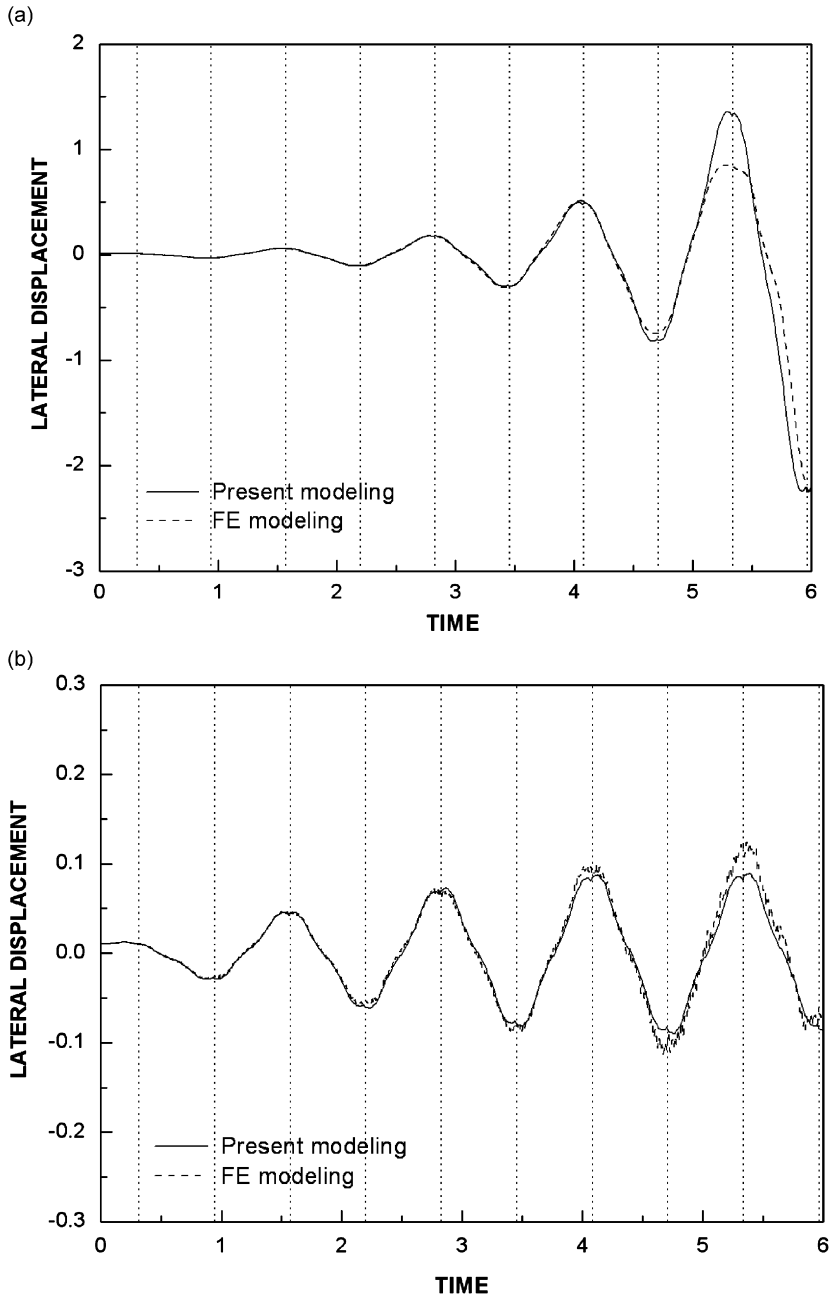

Fig. 15. Impulse magnitude effect on the system response at points C and D (shown in Fig. 13) with $\zeta = 0.1$ and $\gamma = 10$.: (a) point C (1.65, 0.10) and (b) point D (1.65, 1.25).

the modal damping ratio on the stability characteristics of the axially oscillating beam are investigated. Generally, if the impulse magnitude exceeds a certain limit, it will destabilize the system. However, in certain region, a proper amount of impulse magnitude can improve the stability of the system. Finally, as the modal damping ratio increases, the unstable region in the contour map generally decreases. Furthermore, the benefit of imparting periodic impulsive force to stabilize the system can be obtained more effectively with the damping effect.

Acknowledgement

This work was supported by the research fund of Hanyang University (HY-2006-I).

References

[1] M. Faraday, On a peculiar class of acoustical figures and on certain forms assumed by a group of particles upon vibrating elastic surfaces, *Philosophical Transactions of the Royal Society*, London, 1831, pp. 299–318.
[2] E. Mathieu, Memoire sur ie movement vibratoire d'une membrane de forme elliptique, *Journal of Mathematics* 13 (1868) 137–203.
[3] G.W. Hill, On the part of the lunar perigee which is a function of the mean motions of the Sun and Moon, *Acta Mathematica* 8 (1886) 1–36.
[4] A.H. Nayfeh, D.T. Mook, Parametric excitations of linear systems having many degrees of freedom, *Journal of Acoustical Society of America* 62 (1977) 375–381.
[5] T.R. Beal, Dynamic stability of a flexible missile under constant and pulsating thrusts, *AIAA Journal* 3 (1965) 486–494.
[6] E.R. Christensen, S.W. Lee, Non-linear finite element modeling of the dynamics of unrestrained flexible structures, *Computers and Structures* 12 (1986) 708–718.
[7] J.C. Simo, L. Vu-Quoc, On the dynamics of flexible beams under large overall motions-the plane case part I and part II, *Journal of Applied Mechanics* 42 (1986) 738–752.
[8] L.D. Zavodney, A.H. Nayfeh, The non-linear response of a slender beam carrying a lumped mass to a principal parametric excitation: theory and experiment, *International Journal of Non-linear Mechanics* 24 (2) (1989) 105–125.
[9] S.K. Dwivedy, R.C. Kar, Dynamics of a slender beam with an attached mass under combination parametric and internal resonances—part I: steady state response, *Journal of Sound and Vibration* 221 (5) (1999) 823–848.
[10] S.K. Dwivedy, R.C. Kar, Dynamics of a slender beam with an attached mass under combination parametric and internal resonances—part II: periodic and chaotic responses, *Journal of Sound and Vibration* 222 (2) (1999) 281–305.
[11] B. Pratiher, S.K. Dwivedy, Parametric instability of a cantilever beam with magnetic field and periodic axial load, *Journal of Sound and Vibration* 305 (5) (2007) 904–917.
[12] T.R. Kane, R.R. Ryan, A.K. Banerjee, Dynamics of cantilever beam attached to a moving base, *Journal of Guidance, Control and Dynamics* 10 (1987) 139–151.
[13] H.H. Yoo, R.R. Ryan, R.A. Scott, Dynamics of flexible beams undergoing overall motions, *Journal of Sound and Vibration* 181 (1995) 261–278.
[14] S. Seo, H.H. Yoo, Dynamic analysis of flexible beams undergoing overall motion employing linear strain measures, *AIAA Journal* 40 (2) (2002) 319–326.
[15] H.H. Yoo, J. Chung, Dynamics of rectangular plates undergoing prescribed overall motion, *Journal of Sound and Vibration* 239 (1) (2001) 123–137.
[16] H.H. Yoo, S.H. Shin, Vibtation analysis of rotating cantilever beams, *Journal of Sound and Vibration* 212 (5) (1998) 807–828.
[17] H.H. Yoo, S.K. Kim, Free vibration analysis of rotating cantilever plates, *AIAA Journal* 40 (11) (2002) 2188–2196.
[18] S.H. Hyun, H.H. Yoo, Dynamic modeling and stability analysis of axially oscillating cantilever beams, *Journal of Sound and Vibration* 228 (3) (1999) 543–558.
[19] J. Chung, D.H. Jung, H.H. Yoo, Stability analysis for the flap wise motion of a cantilever beam with rotary oscillation, *Journal of Sound and Vibration* 273 (5) (2004) 1047–1062.
[20] T.R. Kane, D.A. Levinson, *Dynamics: Theory and Applications*, McGraw-Hill, New York, 1985.
[21] LS-DYNA 970 Keyword User's Manual 2003, Livermore Software Technology Co.
[22] LS-DYNA Theoretical Manual 2003, Livermore Software Technology Co.